Published in final edited form as:
*Nature*. ; 480(7377): 336–343. doi:10.1038/nature10696.

# Structure of HIV-1 gp120 V1/V2 domain with broadly neutralizing antibody PG9

**Jason S. McLellan**[1,*], **Marie Pancera**[1,*], **Chris Carrico**[2], **Jason Gorman**[1], **Jean-Philippe Julien**[3], **Reza Khayat**[3], **Robert Louder**[1], **Robert Pejchal**[3], **Mallika Sastry**[1], **Kaifan Dai**[1], **Sijy O'Dell**[1], **Nikita Patel**[4], **Syed Shahzad-ul-Hussan**[1,5], **Yongping Yang**[1], **Baoshan Zhang**[1], **Tongqing Zhou**[1], **Jiang Zhu**[1], **Jeffrey C. Boyington**[1], **Gwo-Yu Chuang**[1], **Devan Diwanji**[3], **Ivelin Georgiev**[1], **Young Do Kwon**[1], **Doyung Lee**[1], **Mark K. Louder**[1], **Stephanie Moquin**[1], **Stephen D. Schmidt**[1], **Zhi-Yong Yang**[1], **Mattia Bonsignori**[6], **John A. Crump**[7,8], **Saidi H. Kapiga**[9], **Noel E. Sam**[8,9], **Barton F. Haynes**[6], **Dennis R. Burton**[10,11], **Wayne C. Koff**[12], **Laura M. Walker**[10], **Sanjay Phogat**[12], **Richard Wyatt**[13], **Jared Orwenyo**[14], **Lai-Xi Wang**[14], **James Arthos**[4], **Carole A. Bewley**[5], **John R. Mascola**[1], **Gary J. Nabel**[1], **William R. Schief**[2,10], **Andrew B. Ward**[3], **Ian A. Wilson**[3], and **Peter D. Kwong**[1]

[1]Vaccine Research Center, National Institute of Allergy and Infectious Diseases, National Institutes of Health, Bethesda, Maryland 20892, USA

[2]Department of Biochemistry, University of Washington, Seattle, Washington 98195, USA

[3]Department of Molecular Biology and the Skaggs Institute for Chemical Biology, The Scripps Research Institute, La Jolla, California 92037, USA

[4]Laboratory of Immunoregulation, National Institutes of Allergy and Infectious Diseases, National Institutes of Health, Bethesda, Maryland 20892, USA

[5]Laboratory of Bioorganic Chemistry, National Institute of Diabetes and Digestive and Kidney Diseases, National Institutes of Health, Bethesda, Maryland 20892, USA

[6]The Duke Human Vaccine Institute, Duke University School of Medicine, and Duke University Medical Center, Durham, North Carolina 27710, USA

[7]Division of Infectious Diseases and International Health, Department of Medicine, and Department of Pathology, Duke University Medical Center, Durham, North Carolina 27710, USA

Correspondence and requests for materials should be addressed to P.D.K. (pdkwong@nih.gov).
[*]These authors contributed equally to this work.

Supplementary Information is linked to the online version of the paper at www.nature.com/nature.

**Author Information** Coordinates and structure factors for PG9 Fab in complexes with V1/V2 from CAP45 and ZM109 strains of HIV-1 have been deposited with the Protein Data Bank under accession codes 3U4E and 3U2S, respectively. Coordinates and structure factors for unbound Fab structures of PG9, CH04, CH04H/CH02L (in two lattices) and PGT145 have been deposited with the Protein Data Bank under accession codes, 3U36, 3TCL, 3U46, 3U4B and 3US1, respectively. Reprints and permissions information is available at www.nature.com/reprints. The authors declare no competing financial interests. Readers are welcome to comment on the online version of this article at www.nature.com/nature.

**Author Contributions** J.S.M., M.P., M.S., T.Z., J.Z., J.A., C.A.B., J.R.M., G.J.N., W.R.S., A.B.W., I.A.W. and P.D.K. designed research and analysed the data; J.S.M., M.P., C.C., J.G., J.-P.J., R.K., R.L., R.P., M.S., K.D., S.O'D., N.P., S.S.H., Y.Y., T.Z., J.C.B., G.-Y.C., D.D., I.G., Y.D.K., D.L., M.K.L., S.M., S.D.S., Z.-Y.Y. and B.Z. performed research and are listed in four alphabetical groups: J.S.M. and M.P. performed the majority of research and, with C.C., J.G., J.-P.J., R.K., R.L., R.P. and M.S., determined structures, K.D., S.O'D., N.P., S.S.H., Y.Y., B.Z., T.Z. and J.Z. contributed substantial experiments, J.C.B., G.-Y.C., D.D., I.G., Y.D.K., D.L., M.K.L., S.M., S.D.S. and Z.-Y.Y. contributed supporting research; M.B., J.A.C., S.H.K., N.E.S. and B.F.H. contributed donor 0219 materials; D.R.B., W.C.K. and L.M.W. contributed donor 24 and donor 84 materials and T13 antibody; S.P. and R.W. contributed 16055 gp120; J.O. and L.-X.W. contributed polysaccharides; J.S.M., M.P., G.J.N., I.A.W. and P.D.K. wrote the paper, with all principal investigators providing comments or revisions.

[8]Kilimanjaro Christian Medical Centre and Kilimanjaro Christian Medical College, Tumaini University, Moshi, Tanzania

[9]Kilimanjaro Reproductive Health Programme, Moshi, Tanzania

[10]Department of Immunology and Microbial Science and IAVI Neutralizing Antibody Center, The Scripps Research Institute, La Jolla, California 92037, USA

[11]Ragon Institute of MGH, MIT, and Harvard, Cambridge, Massachusetts 02129, USA

[12]International AIDS Vaccine Initiative (IAVI), New York, New York 10038, USA

[13]IAVI Neutralizing Antibody Center at TSRI, Department of Immunology and Microbial Science, The Scripps Research Institute, La Jolla CA 92037, USA

[14]Institute of Human Virology and Department of Biochemistry & Molecular Biology, University of Maryland School of Medicine, Baltimore, Maryland 21201, USA

## Abstract

Variable regions 1 and 2 (V1/V2) of human immunodeficiency virus-1 (HIV-1) gp120 envelope glycoprotein are critical for viral evasion of antibody neutralization, and are themselves protected by extraordinary sequence diversity and *N*-linked glycosylation. Human antibodies such as PG9 nonetheless engage V1/V2 and neutralize 80% of HIV-1 isolates. Here we report the structure of V1/V2 in complex with PG9. V1/V2 forms a four-stranded β-sheet domain, in which sequence diversity and glycosylation are largely segregated to strand-connecting loops. PG9 recognition involves electrostatic, sequence-independent and glycan interactions: the latter account for over half the interactive surface but are of sufficiently weak affinity to avoid autoreactivity. The structures of V1/V2-directed antibodies CH04 and PGT145 indicate that they share a common mode of glycan penetration by extended anionic loops. In addition to structurally defining V1/V2, the results thus identify a paradigm of antibody recognition for highly glycosylated antigens, which—with PG9—involves a site of vulnerability comprising just two glycans and a strand.

As the sole viral target of neutralizing antibodies, the HIV-1 viral spike has evolved to evade antibody-mediated neutralization (reviewed in ref. 1). V1/V2 of the gp120 component of the viral spike is critical to this evasion. Localized by electron microscopy to a membrane-distal 'cap'[2–5], which holds the spike in a neutralization-resistant conformation, V1/V2 is not essential for entry: its removal, however, renders the virus profoundly sensitive to antibody-mediated neutralization[6–9].

The ~50–90 residues that comprise V1/V2 contain two of the most variable portions of the virus, and roughly 1 in 10 residues of V1/V2 are *N*-glycosylated. Despite the diversity and glycosylation of V1/V2, a number of broadly neutralizing human antibodies have been identified that target this region, including the somatically related antibodies PG9 and PG16, which neutralize 70–80% of circulating HIV-1 isolates[10], antibodies CH01–CH04, which neutralize 40–50%[11], and antibodies PGT141–145, which neutralize 40–80%[12]. These antibodies all share specificity for an *N*-linked glycan at residue 160 in V1/V2 (HXB2 numbering) and show a preferential binding to the assembled viral spike over monomeric gp120 as well as a sensitivity to changes in V1/V2 and some V3 residues. Sera with these characteristics have been identified in a number of HIV-1 donor cohorts, and these quaternary-structure-preferring V1/V2-directed antibodies are among the most common broadly neutralizing responses in infected donors[13,14].

Despite extensive effort, V1/V2 had resisted atomic-level characterization. Here we report crystal structures of the V1/V2 domain of HIV-1 gp120 from strains CAP45 and ZM109 in complexes with the antigen-binding fragment (Fab) of PG9 at 2.19- and 1.80-Å resolution,

respectively. We elucidate how the V1/V2 fold accommodates sequence variation and glycosylation, provide an atomic-level description of the PG9 epitope, and analyse other members of this V1/V2-directed class of broadly neutralizing antibodies to identify conserved features that enable recognition of this key glycopeptide target.

## Structure determination

Variational crystallization[15] of HIV-1 gp120 with V1/V2 was attempted following strategies that were successful for structural determination of other portions of HIV-1 gp120 (refs 15–17); this failed to produce V1/V2-containing crystals suitable for structural analysis (Supplementary Table 1). Because V1/V2 emanates from similar hairpins in core structures of HIV-1 (refs 18–21) and SIV[22] (Supplementary Fig. 1), we hypothesized that a protein scaffold that provided an appropriate hairpin might suitably incorporate and express an ectopic V1/V2 region. We identified six proteins with potentially suitable acceptor β-hairpins that ranged in size from 135 to 741 amino acids. Only the smallest of these could be expressed in transfected 293F cells when scaffolded with V1/V2 (Supplementary Table 2), but it behaved poorly in solution. We identified 11 smaller proteins of 36–87 amino acids in size and designed chimaeric proteins encoding V1/V2 from the YU2 strain of HIV-1 (Supplementary Fig. 2 and Supplementary Table 3). The expressed chimaeric glycoproteins from these smaller scaffolds were mostly soluble, permitting us to characterize them antigenically against a panel of six YU2-specific V1/V2 antibodies (Supplementary Tables 4 and 5). Three of the smaller scaffolded YU2 V1/V2 chimaeras showed reactivity with all six YU2-specific antibodies, and two (Protein Data Bank (PDB) accessions1FD6 (ref. 23) and 1JO8 (ref. 24)) were also recognized by the $\alpha_4\beta_7$ integrin[25], suggesting that they retained biological integrity (Supplementary Table 5 and Supplementary Fig. 3). We next identified strains of gp120 that retained PG9 recognition in the gp120 monomer context, including clade B strain TRJO and clade C strains 16055, CAP45, ZM53 and ZM109 (Supplementary Table 6). We placed V1/V2 sequences (residues 126–196) from these strains into the 1FD6 and 1JO8 scaffolds, and assessed PG9 binding. Notably, affinities of PG9 for 1FD6-ZM109 and 1JO8-ZM109 were only 50-fold and threefold lower than wild-type ZM109 gp120, respectively (Supplementary Fig. 4). Scaffold-V1/V2 heterogeneity was apparent after expression in GnTI$^{-/-}$ cells[26] as was sulphation heterogeneity on antibody PG9 (ref. 27) (Supplementary Fig. 5). We therefore used an on-column selection procedure coupled to on-column protease cleavage of Fab to obtain homogeneous complexes of scaffold-V1/V2 with PG9 (Supplementary Fig. 6).

Two 1FD6-V1/V2 scaffolds were crystallized in complex with PG9. One scaffold contained the V1/V2 region from the CAP45 strain of HIV-1 gp120 with five sites of potential *N*-linked glycosylation. Crystals of this CAP45 construct with the Fab of PG9 diffracted to 2.19 Å, and the structure was refined to an $R_{cryst}$ of 18.2% ($R_{free}$ = 23.4%) (Fig. 1 and Supplementary Table 7). A second scaffold included the V1/V2 region from the ZM109 strain of HIV-1 gp120 with *N*-linked glycans at positions 160 and 173, and asparagine to alanine substitutions at four other potential *N*-linked sites. Crystals of this ZM109 construct with the Fab of PG9 diffracted to 1.80 Å, and the structure was refined to an $R_{cryst}$ of 17.8% ($R_{free}$ = 20.5%) (Supplementary Fig. 7 and Supplementary Table 7).

## Structure of V1/V2

The V1/V2 structure, in the context of scaffold and PG9, folds as four anti-parallel β-strands (labelled A, B, C, D) arranged in (−1, −1, +3) topology[28] (Fig. 2a–d and Supplementary Table 8). Important structural elements such as a hydrophobic core, connecting loops and disulphide bonds cross between each of the four strands, indicating that, biologically, the V1/V2 domain should be considered a single topological entity.

Overall, the four-stranded V1/V2 sheet presents an elegant solution for maintaining a common fold while accommodating V1/V2 diversity and glycosylation. Strands contain mostly conserved residues and are welded in place by inter-strand disulphide bonds (between strand A and neighbouring strands B and D) and extensive hydrogen bonding (between strands A and D and between strands B and C). The two faces of the sheet—concave and convex—have very different characters. The concave face of the sheet is glycan-free and hydrophobic (Fig. 2e), with a cluster of aliphatic and aromatic side chains surrounding the disulphide bond that links strands A and B. This conserved hydrophobic cluster continues onto strand D at the sheet edge, to form a half-exposed hydrophobic core for this domain. The convex face of the sheet is cationic (Fig. 2f), with the main-chain atoms of the conserved strands of the sheet forming stripes on the V1/V2 surface (Fig. 2g) and the *N*-linked glycan 160 situated at its centre (Fig. 2h). In contrast, two strand-connecting loops—emanating from the same end of the sheet—are highly glycosylated and variable in sequence (Fig. 2i). We can now redefine the 'V1 loop' as the residues connecting strands A and B, and the 'V2 loop' as those residues between strands C and D (Fig. 2h, i). Of these, the V1 loop is most variable, ranging in length from ~10–30 residues. The V2 loop is less variable and contains at its start the tripeptide motif recognized by integrin $\alpha_4\beta_7$, the gut homing receptor for HIV-1 (ref. 25).

## PG9–V1/V2 interactions

The most prominent interaction between antibody PG9 and V1/V2 occurs with *N*-linked glycan (Fig. 3, Supplementary Fig. 8 and Supplementary Tables 9 and 10). PG9 grasps the entire 160 glycan (Fig. 3a). Its protruding third complementarity-determining region of the heavy chain (CDR H3) reaches through the glycan shield to contact the protein-proximal *N*-acetyl glucosamine, burying 200 $Å^2$ of total surface area, with Asp 100 and Arg 100B of PG9 making four hydrogen bonds (Fig. 3b, c) (Kabat numbering[29] is used in description of antibody sequences; thus Arg 100B is two residues after Asp 100). Additional hydrogen bonds are made by the base of the CDR H3 (by Asn 100P and by the double-mannose-interacting His 100R) to terminal mannose residues, with Ser 32 and Asp 50 of the light chain contributing three additional hydrogen bonds (Fig. 3b). In sum, a total of 11 hydrogen bonds and over 1,150 $Å^2$ of surface area are buried in the PG9–glycan-160 interface (489 $Å^2$ on PG9 and 670 $Å^2$ on glycan 160), with PG9 contacting 5 of the 7 saccharide moieties of the $Man_5GlcNAc_2$ glycan (Fig. 3c). Similar extensive interactions are observed with residue 160 of CAP45 (Supplementary Fig. 8a–c). The preference of PG9 for a $Man_5GlcNAc_2$ glycan at residue 160 is now clear: a larger glycan would clash with the antibody light chain and a shorter glycan would not stretch between tip and base of the PG9 CDR H3.

Interactions also occur between PG9 and the *N*-linked glycan at residue 156 (CAP45) or residue 173 (ZM109). With CAP45, much of the 156 glycan is ordered, stabilizing six of the seven sugars, including four of the five mannose residues (Supplementary Fig. 8). Hydrogen bonds are observed between the 156 glycan and the side chains of Asn 73 and Tyr 100K of the PG9 heavy chain, and 766 $Å^2$ of total buried surface area (337 $Å^2$ on PG9 and 429 $Å^2$ of glycan). Glycan 156 is not preserved in the ZM109 sequence, in which residue 156 is a histidine (Fig. 2i); an additional site of *N*-linked glycosylation, however, occurs in ZM109 at residue 173, in the middle of strand C. In the ZM109 structure, glycan 173 is in virtually the same spatial location as glycan 156 in the CAP45 structure (Fig. 2h). PG9 binds to the protein-proximal *N*-acetylglucosamine, with Tyr 100K making a hydrogen bond and a total of 189 $Å^2$ surface area buried (Fig. 3b). Notably, substitutions that result in changes in V1/V2 glycans indicate that glycan at 160 is critical for PG9 recognition (Supplementary Table 11), and 156/173 is important (although PG9 recognizes strains of HIV-1 lacking a 156/173 glycan; Supplementary Fig. 9). Many of the changes in the heavy and light chains that allow for glycan recognition occur during affinity maturation (Supplementary Tables 12 and 13),

providing a possible explanation for the observed increase in PG9 (and PG16) breadth and affinity during affinity maturation[30].

In addition to glycan recognition, a strand in the CDR H3 of PG9 forms intermolecular parallel β-sheet-like hydrogen bonds to strand C of V1/V2 (Fig. 3d, e). Strand C is the most variable of the V1/V2 strands, and this sequence-independent means of recognition probably allows for increased recognition breadth. Specific electrostatic interactions are also made between cationic residues of strand C and acidic residues on PG9. Notably, several of these occur with sulphated tyrosines on CDR H3. Because parallel β-strand hydrogen bonding would tend to align main-chain atoms of CDR H3 and strand C, the charged tips of Lys and Arg residues would protrude beyond the standard acidic Asp and Glu side chains, whereas tyrosine sulphates provide a closer match to the side-chain length of basic Lys/Arg residues.

Overall, the structure of PG9 is consistent with published mutational data[10,14] (Supplementary Table 14). Some residues such as Phe 176 are critical because they form part of the hydrophobic core on the concave face of the V1/V2 sheet. Others form direct contacts: for example, the tyrosine sulphate at residue 100H of PG9 interacts with residue 168 when it is an Arg (strain ZM109) or Lys (strain CAP45), but would be repelled by a Glu (as in strain JR-FL); JR-FL is resistant to neutralization by PG9, but becomes sensitive if Glu 168 is changed to Lys[10].

## Quaternary preferences of PG9 and PG16

PG9 and the somatically related PG16 typically recognize the assembled viral spike with higher affinity than monomeric gp120 (ref. 10). For PG9, the average monomeric gp120 affinity, as assessed by ELISA or surface plasmon resonance, was at least tenfold weaker than viral spike affinity, as assessed by neutralization; with PG16, the difference was at least 100-fold (Fig. 4a, Supplementary Tables 6 and 15–17). Such differences are probably greater as the concentration required for neutralization (half-maximum inhibitory concentration, $IC_{50}$) is often higher than the affinity (half-maximum effective concentration, $EC_{50}$, or equilibrium dissociation constant $K_d$). To investigate differences between monomeric and oligomeric contexts, we acquired negatively stained electron microscopy images of PG9 in complex with monomeric gp120 (Fig. 4b, Supplementary Figs 10 and 11). To define the orientation of monomeric gp120, we used the CD4-binding-site-directed antibody T13, for which we defined the crystal structure of gp120-bound T13 Fab at 6-Å resolution (Supplementary Figs 12, 13 and Supplementary Table 18). This structure along with the V1/V2–PG9 structure allowed for the definition of six classes of relative gp120–PG9 orientations, indicating that the position of V1/V2 varies in the monomeric gp120 context. In contrast, prior cryoelectron microscopy results indicate that the position of V1/V2 in the unliganded Env trimer spike is fixed[2–5].

Additionally, we chose to map the antibody paratope by assessing neutralization with arginine mutants. We selected the PG16 paratope for characterization, as its recognition seemed to be both more quaternary-structure preferring (Fig. 4a) and more V3 dependent[10] than that of PG9. We parsed its combining site into 21 surface segments plus one in the framework as a control. Each of these was altered by the introduction of a single arginine mutation, expressed as an immunoglobulin, and assessed for neutralization on a panel of diverse HIV-1 isolates (Supplementary Fig. 14). The resultant ‘arginine-scanning’ mutagenesis revealed a close match to the observed V1/V2 interface for PG9 (Fig. 4c). We also measured the binding of PG9 and PG16 to monomeric gp120 in wild-type and V3-deleted contexts, and observed similar affinities, indicating that—in the context of monomeric gp120—V3 does not have a substantial role in PG9 or PG16 recognition

(Supplementary Fig. 15). Lastly, accumulating data indicate that V1/V2 in the viral spike both shields and interacts with V3 (refs 6–9).

Collectively, these results suggest that the V1/V2–PG9 interaction observed in the scaffolded V1/V2–PG9 crystal structures encompasses much of the PG9/PG16 epitope, and that the structural integrity of this epitope is sensitive to appropriate assembly of the viral spike. We note parenthetically that the ability of the PG9/PG16-recognized epitope to be preferentially present in the assembled viral spike provides a useful strategy to hide this potential site of vulnerability. That is, the site may be preferentially present on the assembled viral spike, but not on shed or other monomeric forms of gp120, which are thought to be the predominant form of Env in infected individuals, and we note in this regard that many V1/V2-directed antibodies are substantially more quaternary-structure preferring than PG9 (refs 10–12, 31). The quaternary-specific nature of the epitope may thus reflect a functional adaptation of HIV-1.

## A conserved CDR H3 motif for V1/V2 recognition

Sequences of other V1/V2-directed broadly neutralizing antibodies indicate the presence of long CDR H3s, but little other sequence conservation (Fig. 5a). We have not yet been able to determine structures of other class members in complex with V1/V2, but nonetheless sought to provide insight into their conserved features of recognition by analysing unbound Fab structures.

The structure of unbound PG9 Fab (3.3- Å resolution, four molecules per asymmetric unit; Supplementary Fig. 16 and Supplementary Table 19) revealed considerable CDR H3 flexibility, similar to that observed previously with PG16 (ref. 30). For CH01 CH04 antibodies[11], crystallization was attempted for antigen-binding fragments and for six heavy/light-chain somatic chimaeras (Supplementary Table 20). Structures were determined for CH04 Fab and also for the CH04H/CH02L Fab, the latter in two different crystal forms (Supplementary Fig. 17 and Supplementary Table 19). These structures revealed an anionic CDR H3 for CH04, which extended above the rest of the combining site in a manner similar to the CDR H3s of PG9 and PG16 (Fig. 5b). With CH04, however, the extended hairpin was twisted ~90°, to an orientation that bisected heavy and light chains. The spacing between the protruding CDR H3 and the rest of the combining region was reduced by 8 Å relative to that of PG9, and no CDR H3 tyrosine sulphation was observed.

With PGT141–145 antibodies[12], Fab crystals of unbound PGT145 diffracted to 2.3 Å and revealed an extended, tyrosine-sulphated CDR H3 loop, which, like those of PG9, PG16 and CH04, reached substantially beyond the rest of the CDR loops. In contrast, the β-hairpin of CDR H3 extended vertically (parallel to the long axis of the Fab) (Fig. 5b, Supplementary Fig. 18 and Supplementary Table 19) and was rigidified by extensive tyrosine stacking (along with the standard strand–strand hydrogen bonding). Its negatively charged tip (including two sulphated tyrosines) was followed by a Gly-containing potential ‘hinge’ and resembled an extended version of the CDR H3 of antibody 2909 (refs 32, 33), a highly quaternary-structure-sensitive antibody[31,34] that recognizes an immunotype variant of the V1/V2 target site in which a Lys is substituted for the *N*-linked glycan at position 160 (ref. 35).

Thus, despite having been derived from three different individuals, antibodies from this class of V1/V2-directed broadly neutralizing antibodies all showed anionic protruding CDR H3s (Fig. 5b), most of which were tyrosine sulphated. All also displayed β-hairpins, and although these varied substantially in orientation relative to the rest of the combining site, all appeared capable of penetrating an *N*-linked glycan shield to reach a cationic protein surface.

## A V1/V2 site of HIV-1 vulnerability

With both CAP45 and ZM109 strains of gp120, the V1/V2 site recognized by PG9 consists primarily of two glycans and a strand (Fig. 6a). Minor interaction with strand B and with the B–C connecting loop (3% and 3–5% of the total interactive surface, respectively) complete the epitope, with the entire PG9-recognized surface of V1/V2 contained within the B–C hairpin (Supplementary Table 21). The minimal nature of this epitope suggests that it might be easier to engineer and to present to the immune system than other, more complex, epitopes. The epitopes for antibodies b12 and VRC01, for example, are comprised of seven and six independent protein segments[19,36], respectively. The presence in the PG9 epitope of *N*-linked glycosylation, which is added by host cell machinery, does provide a potentially complicating factor for humoral recognition.

To assess glycan affinities, we used saturation transfer difference NMR. In the crystal structure, recognition by PG9 occurs with protein-proximal *N*-acetylglucosamine and terminal mannose saccharides. With 1.5 mM (*N*-acetylglucosamine)$_2$, interaction with PG9 was not observed (Supplementary Fig. 19), whereas with 1.5 mM oligomannose-5, weak interactions were observed (Supplementary Fig. 20). We further carried out a titration series with Asn-(*N*-actylglucosamine)$_2$(mannose)$_5$ and determined its affinity for PG9 to be 1.6 ± 0.9 mM (Fig. 6b). The weak affinity for glycan (surprising in the face of such a large contact surface and multiple hydrogen bonds) provides a potential explanation for the reported lack of PG9 autoreactivity despite its *N*-glycan dependence[10] (specificity for oligomannose-5 probably also reduces PG9 autoreactivity, as this glycan is infrequently displayed on the surface of mammalian cells).

Strand C is the most cationic of the V1/V2 strands. This conserved cationic character—present in the target-cell-facing V1/V2 cap of the viral spike—may relate to the observed anionic interactions of the viral spike, both with dextran sulphate[37,38] and other polyanions[39,40] or with heparan sulphate on the cell surface[41]. In terms of the ionic interactions of PG9 itself, we observed sulphation to increase affinity and neutralization potency by ~10-fold[10,27] (Supplementary Fig. 5). Ionic PG9 interactions may thus mimic the functional polyanion V1/V2 interactions that HIV-1 uses for cell surface attachment during the initial stages of virus cell entry.

Strand C is also the most variable of the V1/V2 strands. Its location, at the edge of the sheet, however, provides an opportunity for sequence-independent recognition, through its exposed main-chain atoms. Whereas the four hydrogen bonds made by the main chain of PG9 probably contribute only a small portion of the overall binding energy, the surface of V1/V2 involved in main-chain interactions with PG9 totals 348 and 350 Å$^2$ in the CAP45 and ZM109 complexes, respectively, potentially providing a substantial contribution to the overall binding energy (Supplementary Table 21). This type of β-sheet interaction, for example, is the primary interaction between the CDR H3 of antibody 447-52D with the V3 of gp120 (ref. 42) in a 3-and-almost-4-stranded β-sheet.

## Vaccine implications

The different types of PG9 interaction, involving glycan, electrostatic and sequence-independent interactions, all seem to be necessary for PG9 function. Such multicomponent recognition may also provide a mechanism that enables the immune system to overcome evasion associated with individual components of the interaction. Thus, for example, glycan-only affinity might lead to autoreactivity, and surface areas of electrostatic and sequence-independent interactions might be individually too small to generate sufficient affinity for tight interactions. Together, however, the glycan, electrostatic and sequence-

independent interactions achieve the substantial level of affinity required for potent neutralization.

In longitudinal studies, antibody responses that require glycan, either at residue 160, as described here, or at residue 332, constitute the most commonly elicited initial broadly neutralizing responses[43], an observation also seen with elite neutralizers[13]. In such studies, transmitted/founder viruses in some cases did not show canonical glycosylation (for example, at positions 160 or 332), but acquired these under immune selection[44]. Thus it seems that *N*-linked glycosylation at particular residues is selected as a means of immune evasion, but that these same glycans—now part of a homogeneous glycan array—can be recognized by very broadly neutralizing antibodies. Recent structural results indicate that a number of 332-glycan-dependent antibodies also use protruding CDR H3s and, in at least one case, the antibody (PGT128) recognizes an epitope composed of two glycans and a strand[45]. Collectively these results suggest that a penetrating CDR H3 that recognizes a conserved glycan and neighbouring polypeptide is a paradigm for humoral recognition of heavily glycosylated antigens.

Lastly, we note that recent immune analyses of the RV144 vaccine trial suggest that the presence of V1/V2-reactive antibodies associates inversely with HIV-1-infection risk[46,47]. What role these antibodies play in protection, however, is unknown. It is nonetheless fascinating that the V1/V2 domain—which functions in evading antibody-mediated neutralization—is itself a site of effective neutralization by a number of broadly neutralizing antibodies (for example, by PG9, CH04 and PGT145) and that antibodies against this domain seem to be an indicator of a successful vaccine outcome.

## METHODS SUMMARY

Proteins that could accommodate backbone grafting of the V1/V2 stub from HIV-1 gp120 were identified using the Multigraft Match algorithm[48] implemented in Rosetta. Potential V1/V2 scaffolds were examined manually and, if necessary, optimizations were made to accommodate full-length V1/V2 loops (residues 126–196) or to alter scaffold properties (for example, mutating the intrinsic immunoglobulin affinity of 1FD6; ref. 49). For each V1/V2 scaffold, protein-A-purified PG9, altered to remove light-chain glycosylation and to introduce an HRV3C cleavage site in the hinge, was bound to Protein A Plus agarose, and the V1/V2 scaffold added. After washing away unbound scaffold, HRV3C protease was added to elute the PG9 Fab–V1/V2 scaffold complex. Complexes of PG9 Fab bound to 1FD6-CAP45 or 1FD6-ZM109 crystallized in similar conditions[50] (8–17% (w/v) PEG 3350, 5–10% (v/v) 2-methyl-2,4-pentanediol, 0.2 M lithium sulphate, 0.1 M imidazole pH 6.5). Crystals were cryoprotected with 15% (v/v) 2R,3R-butanediol, diffraction data were collected to 2.19 and 1.80 Å for PG9–1FD6-CAP45 and PG9–1FD6-ZM109, respectively, and structures solved by molecular replacement.

## Supplementary Material

Refer to Web version on PubMed Central for supplementary material.

## Acknowledgments

We thank A. Changela and X. Wu for assistance with mapping the PG16 paratope, J. Sodroski for discussions, J. Stuckey for assistance with figures, and members of the Structural Biology Section and Structural Bioinformatics Core, Vaccine Research Center, for discussions and comments on the manuscript. Support for this work was provided by the Intramural Research Program of the National Institutes of Health (NIH), by the International AIDS Vaccine Initiative, by the Ragon Institute, by the Canadian Institute of Health Research and by grants from the NIH. The three-dimensional reconstructions were conducted at the National Resource for Automated Molecular Microscopy (NRAMM), which is supported by the NIH through the National Center for Research Resources' P41

program (RR017573). Use of sector 22 (Southeast Region Collaborative Access team) at the Advanced Photon Source was supported by the US Department of Energy, Basic Energy Sciences, Office of Science, under contract number W-31-109-Eng-38.

## References

1. Wyatt R, Sodroski J. The HIV-1 envelope glycoproteins: fusogens, antigens, and immunogens. Science. 1998; 280:1884–1888. [PubMed: 9632381]
2. Liu J, Bartesaghi A, Borgnia MJ, Sapiro G, Subramaniam S. Molecular architecture of native HIV-1 gp120 trimers. Nature. 2008; 455:109–113. [PubMed: 18668044]
3. Wu SR, et al. Single-particle cryoelectron microscopy analysis reveals the HIV-1 spike as a tripod structure. Proc Natl Acad Sci USA. 2010; 107:18844–18849. [PubMed: 20956336]
4. White TA, et al. Molecular architectures of trimeric SIV and HIV-1 envelope glycoproteins on intact viruses: strain-dependent variation in quaternary structure. PLoS Pathog. 2010; 6:e1001249. [PubMed: 21203482]
5. Hu G, Liu J, Taylor KA, Roux KH. Structural comparison of HIV-1 envelope spikes with and without the V1/V2 loop. J Virol. 2011; 85:2741–2750. [PubMed: 21191026]
6. Cao J, et al. Replication and neutralization of human immunodeficiency virus type 1 lacking the V1 and V2 variable loops of the gp120 envelope glycoprotein. J Virol. 1997; 71:9808–9812. [PubMed: 9371651]
7. Stamatatos L, Cheng-Mayer C. An envelope modification that renders a primary, neutralization-resistant clade B human immunodeficiency virus type 1 isolate highly susceptible to neutralization by sera from other clades. J Virol. 1998; 72:7840–7845. [PubMed: 9733820]
8. Pinter A, et al. The V1/V2 domain of gp120 is a global regulator of the sensitivity of primary human immunodeficiency virus type 1 isolates to neutralization by antibodies commonly induced upon infection. J Virol. 2004; 78:5205–5215. [PubMed: 15113902]
9. Rusert P, et al. Interaction of the gp120 V1/V2 loop with a neighboring gp120 unit shields the HIV envelope trimer against cross-neutralizing antibodies. J Exp Med. 2011; 208:1419–1433. [PubMed: 21646396]
10. Walker LM, et al. Broad and potent neutralizing antibodies from an African donor reveal a new HIV-1 vaccine target. Science. 2009; 326:285–289. [PubMed: 19729618]
11. Bonsignori M, et al. Analysis of a clonal lineage of HIV-1 envelope V2/V3 conformational epitope-specific broadly neutralizing antibodies and their inferred unmutated common ancestors. J Virol. 2011; 85:9998–10009. [PubMed: 21795340]
12. Walker LM, et al. Broad neutralization coverage of HIV by multiple highly potent antibodies. Nature. 2011; 477:466–470. [PubMed: 21849977]
13. Walker LM, et al. A limited number of antibody specificities mediate broad and potent serum neutralization in selected HIV-1 infected individuals. PLoS Pathog. 2010; 6:e1001028. [PubMed: 20700449]
14. Moore PL, et al. Potent and broad neutralization of HIV-1 subtype C by plasma antibodies targeting a quaternary epitope including residues in the V2 loop. J Virol. 2011; 85:3128–3141. [PubMed: 21270156]
15. Kwong PD, et al. Probability analysis of variational crystallization and its application to gp120, the exterior envelope glycoprotein of type 1 human immunodeficiency virus (HIV-1). J Biol Chem. 1999; 274:4115–4123. [PubMed: 9933605]
16. Huang CC, et al. Structure of a V3-containing HIV-1 gp120 core. Science. 2005; 310:1025–1028. [PubMed: 16284180]
17. Pancera M, et al. Structure of HIV-1 gp120 with gp41-interactive region reveals layered envelope architecture and basis of conformational mobility. Proc Natl Acad Sci USA. 2010; 107:1166–1171. [PubMed: 20080564]
18. Kwong PD, et al. Structure of an HIV gp120 envelope glycoprotein in complex with the CD4 receptor and a neutralizing human antibody. Nature. 1998; 393:648–659. [PubMed: 9641677]
19. Zhou T, et al. Structural definition of a conserved neutralization epitope on HIV-1 gp120. Nature. 2007; 445:732–737. [PubMed: 17301785]

20. Chen L, et al. Structural basis of immune evasion at the site of CD4 attachment on HIV-1 gp120. Science. 2009; 326:1123–1127. [PubMed: 19965434]
21. Kwong PD, et al. Structures of HIV-1 gp120 envelope glycoproteins from laboratory-adapted and primary isolates. Structure. 2000; 8:1329–1339. [PubMed: 11188697]
22. Chen B, et al. Structure of an unliganded simian immunodeficiency virus gp120 core. Nature. 2005; 433:834–841. [PubMed: 15729334]
23. Ross SA, Sarisky CA, Su A, Mayo SL. Designed protein G core variants fold to native-like structures: sequence selection by ORBIT tolerates variation in backbone specification. Protein Sci. 2001; 10:450–454. [PubMed: 11266631]
24. Fazi B, et al. Unusual binding properties of the SH3 domain of the yeast actin-binding protein Abp1: structural and functional analysis. J Biol Chem. 2002; 277:5290–5298. [PubMed: 11668184]
25. Arthos J, et al. HIV-1 envelope protein binds to and signals through integrin $\alpha_4\beta_7$, the gut mucosal homing receptor for peripheral T cells. Nature Immunol. 2008; 9:301–309. [PubMed: 18264102]
26. Reeves PJ, Callewaert N, Contreras R, Khorana HG. Structure and function in rhodopsin: high-level expression of rhodopsin with restricted and homogeneous *N*-glycosylation by a tetracycline-inducible *N*-acetylglucosaminyltransferase I-negative HEK293S stable mammalian cell line. Proc Natl Acad Sci USA. 2002; 99:13419–13424. [PubMed: 12370423]
27. Pejchal R, et al. Structure and function of broadly reactive antibody PG16 reveal an H3 subdomain that mediates potent neutralization of HIV-1. Proc Natl Acad Sci USA. 2010; 107:11483–11488. [PubMed: 20534513]
28. Richardson JS. The anatomy and taxonomy of protein structure. Adv Protein Chem. 1981; 34:167–339. [PubMed: 7020376]
29. Kabat, EA.; Wu, TT.; Perry, HM.; Gottesman, KS.; Foeller, C. Sequences of Proteins of Immunological Interest. 5. US Department of Health and Human Service, National Institutes of Health; 1991.
30. Pancera M, et al. Crystal structure of PG16 and chimeric dissection with somatically related PG9: structure function analysis of two quaternary-specific antibodies that effectively neutralize HIV-1. J Virol. 2010; 84:8098–8110. [PubMed: 20538861]
31. Gorny MK, et al. Identification of a new quaternary neutralizing epitope on human immunodeficiency virus type 1 virus particles. J Virol. 2005; 79:5232–5237. [PubMed: 15795308]
32. Changela A, et al. Crystal structure of human antibody 2909 reveals conserved features of quaternary structure-specific antibodies that potently neutralize HIV-1. J Virol. 2011; 85:2524–2535. [PubMed: 21191009]
33. Spurrier B, et al. Structural analysis of human and macaque mAbs 2909 and 2.5B: implications for the configuration of the quaternary neutralizing epitope of HIV-1 gp120. Structure. 2011; 19:691–699. [PubMed: 21565703]
34. Honnen WJ, et al. Type-specific epitopes targeted by monoclonal antibodies with exceptionally potent neutralizing activities for selected strains of human immunodeficiency virus type 1 map to a common region of the V2 domain of gp120 and differ only at single positions from the clade B consensus sequence. J Virol. 2007; 81:1424–1432. [PubMed: 17121806]
35. Wu X, et al. Immunotypes of a quaternary site of HIV-1 vulnerability and their recognition by antibodies. J Virol. 2011; 85:4578–4585. [PubMed: 21325411]
36. Zhou T, et al. Structural basis for broad and potent neutralization of HIV-1 by antibody VRC01. Science. 2010; 329:811–817. [PubMed: 20616231]
37. Mitsuya H, et al. Dextran sulfate suppression of viruses in the HIV family: inhibition of virion binding to CD4+ cells. Science. 1988; 240:646–649. [PubMed: 2452480]
38. Schols D, Pauwels R, Desmyter J, De Clercq E. Dextran sulfate and other polyanionic anti-HIV compounds specifically interact with the viral gp120 glycoprotein expressed by T-cells persistently infected with HIV-1. Virology. 1990; 175:556–561. [PubMed: 1691563]
39. Moulard M, et al. Selective interactions of polyanions with basic surfaces on human immunodeficiency virus type 1 gp120. J Virol. 2000; 74:1948–1960. [PubMed: 10644368]

40. Fletcher PS, Wallace GS, Mesquita PM, Shattock RJ. Candidate polyanion microbicides inhibit HIV-1 infection and dissemination pathways in human cervical explants. Retrovirology. 2006; 3:46. [PubMed: 16882346]
41. Mondor I, Ugolini S, Sattentau QJ. Human immunodeficiency virus type 1 attachment to HeLa CD4 cells is CD4 independent and gp120 dependent and requires cell surface heparans. J Virol. 1998; 72:3623–3634. [PubMed: 9557643]
42. Stanfield RL, Gorny MK, Williams C, Zolla-Pazner S, Wilson IA. Structural rationale for the broad neutralization of HIV-1 by human monoclonal antibody 447-52D. Structure. 2004; 12:193–204. [PubMed: 14962380]
43. Gray ES, et al. The neutralization breadth of HIV-1 develops incrementally over four years and is associated with CD4 T cell decline and high viral load during acute infection. J Virol. 2011; 85:4828–4840. [PubMed: 21389135]
44. Moore PL, et al. Evolution of HIV-1 transmitted/founder viruses results in the formation of epitopes for later broadly cross-neutralizing antibodies. AIDS Res Hum Retroviruses. 2011; 27:A-29.
45. Pejchal R, et al. A potent and broad neutralizing antibody recognizes and penetrates the HIV glycan shield. Science. Oct 13.2011 10.1126/science.1213256
46. Karasavvas N, et al. The Thai Phase III clinical trial (RV144) induces the generation of antibodies that target a conserved region within the V2 loop of gp120. AIDS Res Hum Retroviruses. 2011; 27:A-29.
47. Zolla-Pazner S, et al. V2-reactive antibodies in RV144 vaccinees' plasma. AIDS Res Hum Retroviruses. 2011; 27:A-21.
48. Azoitei ML, et al. Computation-guided backbone grafting of a discontinuous motif onto a protein scaffold. Science. 2011; 334:373–376. [PubMed: 22021856]
49. Sloan DJ, Hellinga HW. Dissection of the protein G B1 domain binding site for human IgG Fc fragment. Protein Sci. 1999; 8:1643–1648. [PubMed: 10452608]
50. Majeed S, et al. Enhancing protein crystallization through precipitant synergy. Structure. 2003; 11:1061–1070. [PubMed: 12962625]

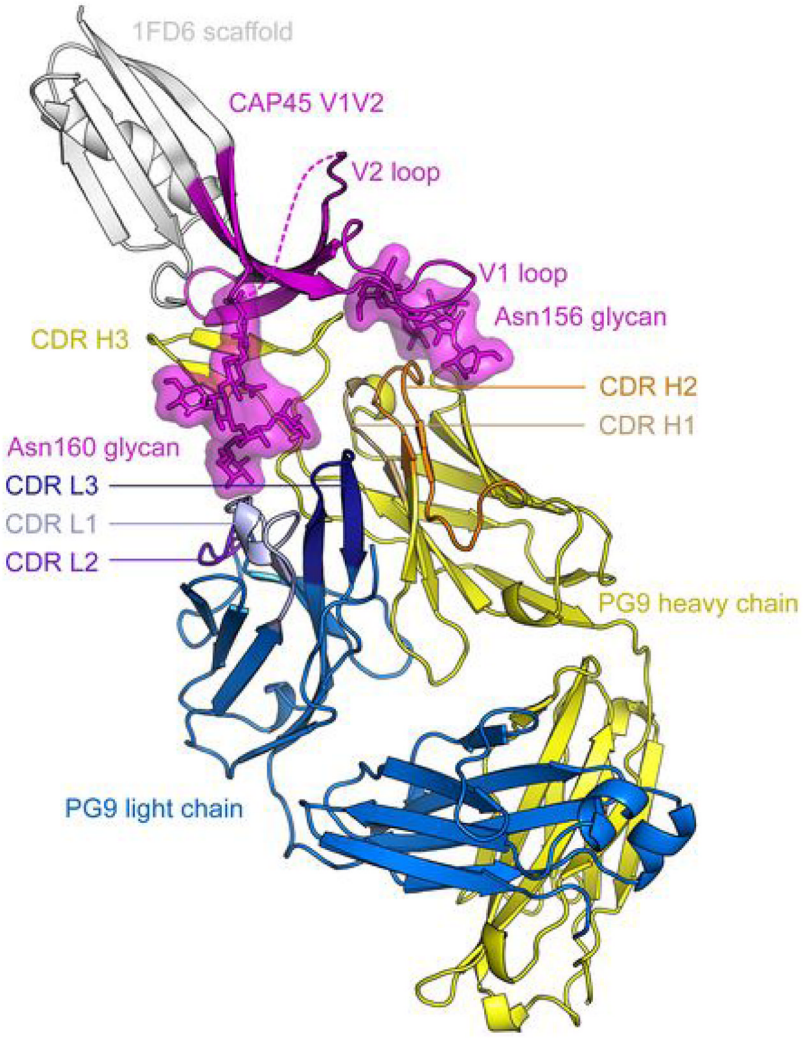


**Figure 1. Overall structure of the V1/V2 domain of HIV-1 gp120 in complex with PG9**

V1/V2 from the CAP45 strain of HIV-1 is shown, in magenta ribbons, in complex with Fab of antibody PG9. The PG9 heavy and light chains are shown as yellow and blue ribbons, respectively, with CDRs in different shades. Although the rest of HIV-1 gp120 has been replaced by the 1FD6 scaffold (shown in white ribbons), the positions of V1/V2, PG9 and the scaffold are consistent with the proposal that the viral spike, and hence the viral membrane, is positioned towards the top of the page. The extended CDR H3 of PG9 is able to penetrate the glycan shield that covers the V1/V2 cap on the spike and to reach conserved elements of polypeptide, while residues in heavy- and light-chain-combining regions recognize *N*-linked glycans. The disordered region of the V2 loop is represented by a dashed line. Perpendicular views of V1/V2 are shown in Figs 2 and 6, and the structure of PG9 in complex with V1/V2 from HIV-1 strain ZM109 is shown in Supplementary Fig. 7.

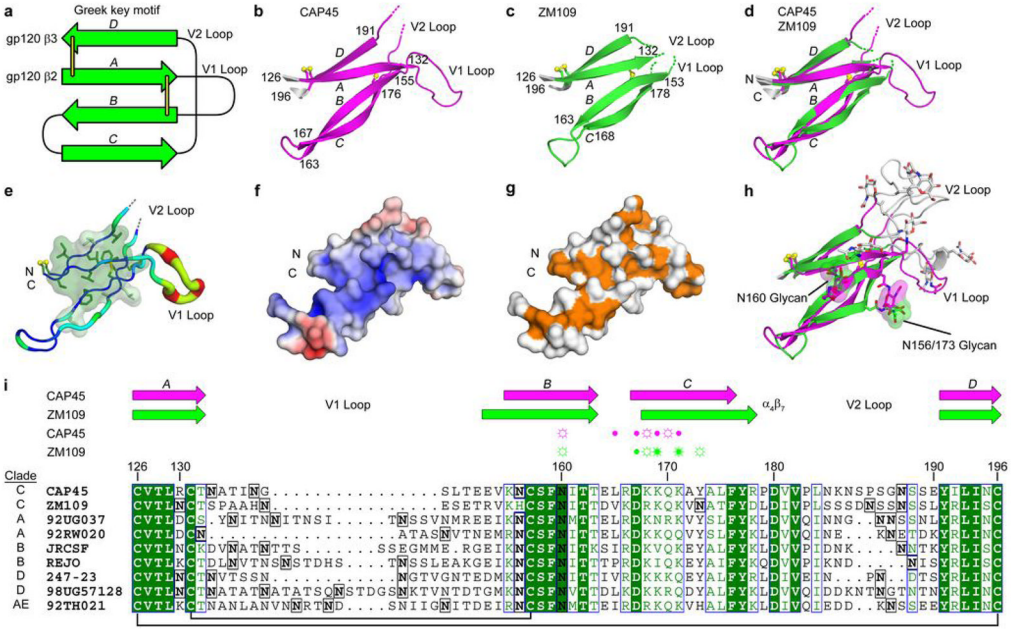


**Figure 2. Structure of the V1/V2 domain of HIV-1 gp120**

**a–i**, The four anti-parallel strands that define V1/V2 fold as a single domain, in a topology known as ‘Greek key’ that is observed in many proteins. **a**, Schematic of V1/V2 topology. V1/V2 resides between strands β2 and β3 of core gp120, and its structure completes the crystallographic determination of all portions of HIV-1 gp120. Strands are depicted as arrows and disulphide bonds as yellow lines. **b**, **c**, Ribbon diagram of V1/V2 residues 126–196 from HIV-1 strains CAP45 (magenta) and ZM109 (green). Conserved disulphide bonds are represented as ball and stick, and the beginning and terminating residues of each strand are labelled. **d**, Superposition of the structures shown in **b** and **c. e**, Amino acid conservation of V1/V2. The backbone is shown as a tube of variable thickness, coloured as a rainbow from cold (blue) to hot (red), corresponding to conserved (thin) and to variable (thick), respectively, based on an alignment of 166 HIV-1 sequences. Aliphatic and aromatic side chains are shown as sticks with semi-transparent molecular surface, coloured by conservation as in **i. f**, Electrostatic surface potentials of CAP45 V1/V2 coloured blue to red, corresponding to positive and negative surface potentials, respectively. **g**, Molecular surfaces corresponding to main-chain atoms including $C_\beta$ are coloured orange, with other surfaces coloured white. **h**, Superposition of ZM109 and CAP45 models containing V1 and V2 loops and associated glycans. For each glycosylated asparagine, only the first *N*-acetylglucosamine attached to the asparagine is shown and represented as sticks with a transparent molecular surface. Modelled amino acids and glycans that are disordered in the crystal structures are shown in grey. **i**, Sequence alignment of nine HIV-1 strains that are potently neutralized by PG9. Glycosylated asparagine residues are boxed and in bold. Identical residues have a dark green background with white characters, whereas conserved residues have white backgrounds with dark green characters. Above the alignment, β-strands are shown as arrows, coloured magenta and green for CAP45 and ZM109, respectively. Residues and attached glycans that make hydrogen bonds to PG9 are denoted with symbols above the alignment (side-chain hydrogen bonds are indicated by open circles with dashes, main-chain hydrogen bonds are indicated by closed circles, or both).

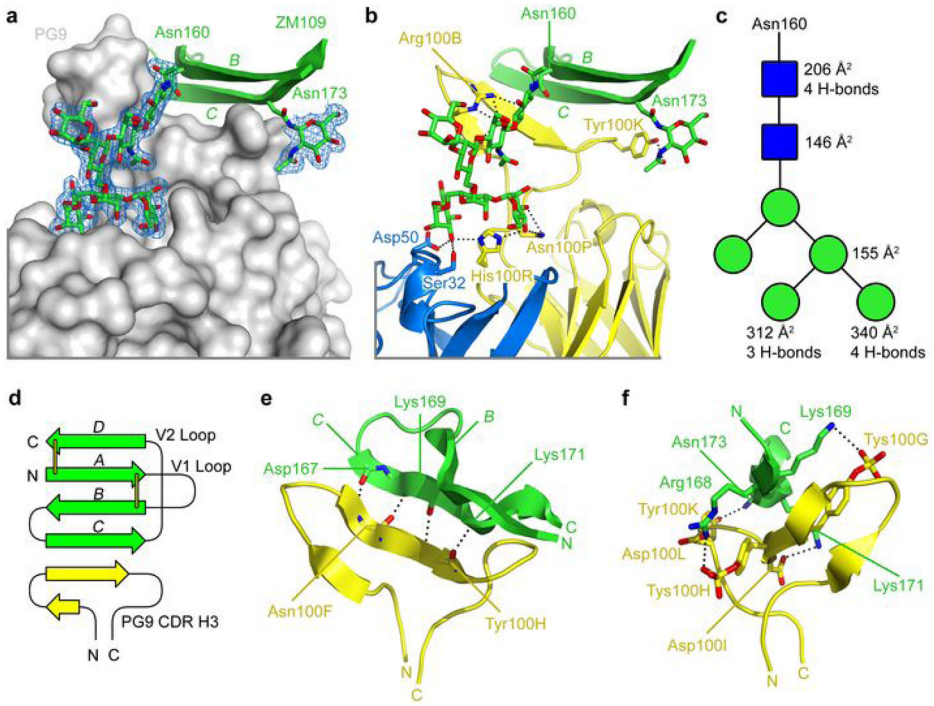


**Figure 3. PG9 V1/V2 interactions**

**a–f**, Glycan, electrostatic and sequence-independent interactions of antibody PG9 facilitate recognition of V1/V2 from the ZM109 strain of HIV-1 gp120. **a**, PG9 is shown as a grey molecular surface, and strands B and C of V1/V2 are shown as green ribbons. Mannose and *N*-acetylglucosamine residues are shown in stick representation, as are the side chains of Asn 160 and 173. Electron density ($2F_o-F_c$) is contoured at 1**σ** and shown as a blue mesh. **b**, Ribbon representations of strands B and C of ZM109 V1/V2 (green), PG9 heavy chain (yellow) and PG9 light chain (blue). V1/V2 glycans and PG9 residues that hydrogen bond are shown as sticks. Nitrogen atoms are coloured blue, oxygen atoms are coloured red, and dotted lines represent hydrogen bonds. **c**, Schematic of the $Man_5GlcNac_2$ moiety attached to Asn 160. GlcNacs are shown as blue squares, and mannoses as green circles. Hydrogen bonds to PG9 are listed to the right of the symbols, as is the total surface area buried at the interface between PG9 and each sugar. **d**, Schematic of the PG9–main-chain interaction with V1/V2. Disulphide bonds in V1/V2 are shown as yellow sticks. **e**, **f**, Ribbon representation of V1/V2 (green) and PG9 CDR H3 (yellow). Hydrogen bonds are represented by dotted lines. Main-chain interactions are shown in **e**, and side chain interactions in **f** (with the two images related by a 90° rotation about a vertical axis). Details of the PG9 interaction with V1/V2 from the CAP45 strain of HIV-1 are shown in Supplementary Fig. 8.

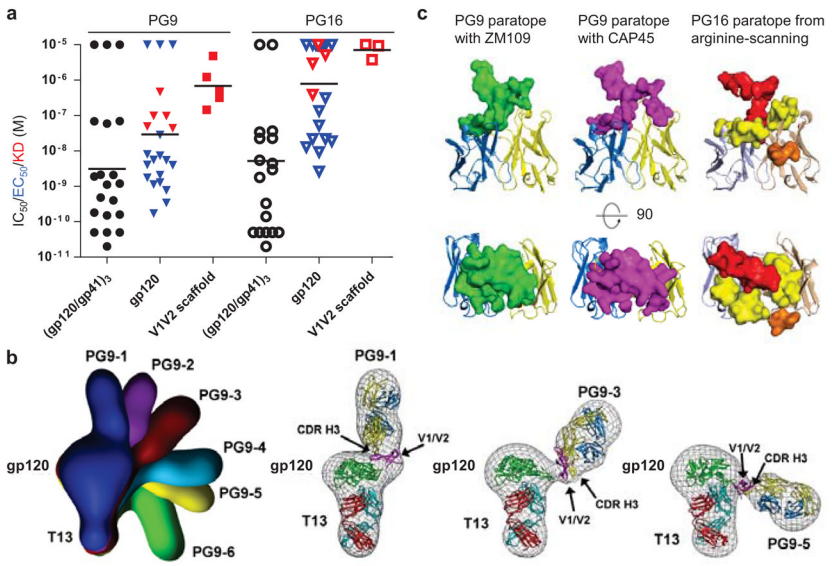


**Figure 4. PG9 and PG16 recognition of the HIV-1 viral spike, monomeric gp120 and scaffolded V1/V2**

**a–c**,Quaternary-structure-preferring antibodies show different affinities for oligomeric, monomeric and scaffolded V1/V2. Both structural and arginine-scanning mapping, however, suggest that the epitopes of PG9 and PG16 are mostly present in scaffolded V1/V2. **a**, Affinities of PG9 (filled symbols) and PG16 (open symbols) are shown for the functional viral spike $(gp120/gp41)_3$ (circles), monomeric gp120 (triangles), and scaffold-V1/V2 (squares), based on neutralization (black), ELISA (blue) and surface plasmon resonance (red). **b**, Negative stained images are shown for ternary complexes of wild-type gp120 (HIV-1 strain 16055) in complex with antibody PG9 and the CD4-binding-site antibody T13. Six different classifications were observed, and are superimposed in the top left panel and labelled PG9-1 to PG9-6. Individual fitting for classes PG9-1, PG9-3 and PG9-5 are shown after rigid-body alignment of Fab PG9–scaffold-V1/V2, Fab T13 and core gp120 (in the conformation bound by the CD4-binding site antibody F105; ref. 20). **c**, Comparison of crystallographically defined PG9 paratope with neutralization-defined PG16 paratope. Scaffold-V1/V2 interactive surface of PG9 in ZM109 (left) and CAP45 (middle) contexts is shown along with the PG16 paratope (right) as defined by arginine-scanning mutagenesis (orange-highlighted residue is Trp 64 in the CDR H2). Perpendicular views of the paratope, rotated by 90° about a horizontal axis, are shown in top and bottom rows.

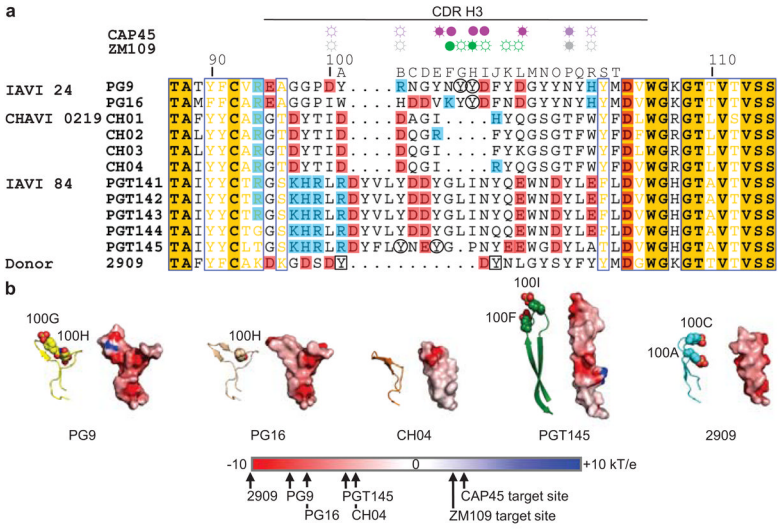


**Figure 5. CDR H3 features of V1/V2-directed broadly neutralizing antibodies**

**a**, **b**, A protruding anionic CDR H3 is preserved in members of this broadly neutralizing class of antibodies. **a**, CDR H3 sequence alignment. Cohort, donor information and sequences in the CDR H3 (Kabat[29] definition and numbering) are shown for V1/V2-directed antibodies. Positively charged residues are boxed in blue and negatively charged residues in red. Residues that make hydrogen bonds to CAP45 residues (magenta) or glycans (purple) are denoted with symbols above the alignment (side-chain hydrogen bonds are indicated by open circles with dashes, main-chain hydrogen bonds by closed circles, or both). Similar contacts are shown for ZM109 residues (green) or glycans (grey). Sulphated tyrosines are circled or squared if the post-translational modification has been confirmed crystallographically or by mass spectrometry, respectively. The sequence for the V1/V2-directed strain-specific antibody, 2909, is also included. **b**, Protruding CDR H3, displayed as ribbon diagrams with sulphated tyrosines shown in spheres and paired with electrostatic surface potentials coloured blue to red, corresponding to positive and negative surface potentials, respectively. All CDR H3s are aligned so that the light chain would be on the left and the heavy chain on the right (as in Supplementary Fig. 17). Average electrostatic potentials are shown for specified CDR H3 and V1V2 surfaces.

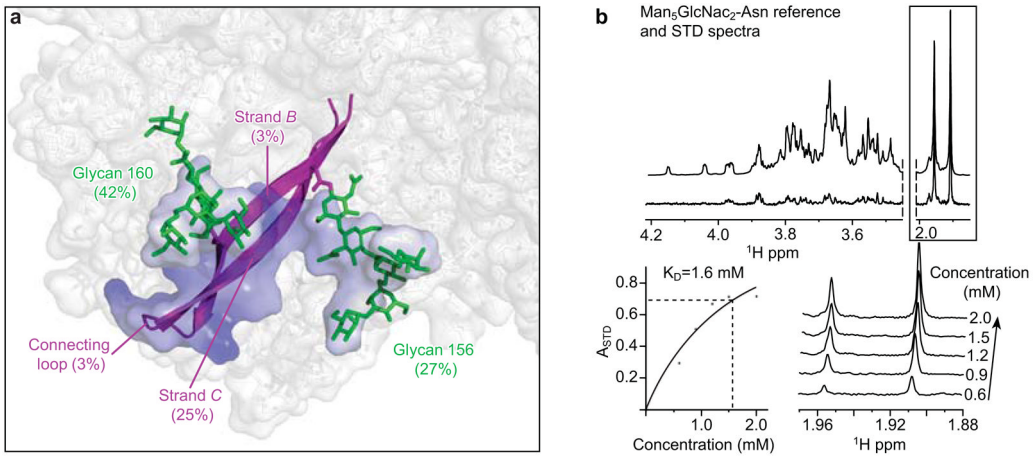


**Figure 6. Two glycans and a strand comprise a V1/V2 site of vulnerability**

**a**, **b**, Glycan, electrostatic and sequence-independent interactions allow PG9 to recognize a glycopeptide site on V1/V2. **a**, Site characteristics in CAP45 strain of HIV-1. Glycans 160 and 156 (173 with ZM109) are highlighted in green, and strands B and C are highlighted in magenta, with the rest of V1/V2 in semi-transparent white. The interactive surface of V1/V2 with PG9 is shown, coloured according to the local electrostatic potential as in Fig. 5b. The contribution of each structural element to that surface is provided as a percentage of the total. Although the V1/V2 scaffolds used here do not allow a comprehensive analysis of the overall antibody response to this region of gp120, in addition to assisting with structural definition of effective V1/V2-directed neutralization, the V1/V2 scaffolds may have utility in attempts to direct the V1/V2-elicited response away from the hypervariable loops to the conserved strands—especially the site of vulnerability highlighted here. **b**, Saturation transfer difference (STD) NMR for $Man_5GlcNAc_2$-Asn binding to PG9. Top, STD spectrum of 1.5 mM $Man_5GlcNAc_2$-Asn in the presence of 15 μM Fab PG9 (lower spectrum) is paired with the corresponding reference spectrum (upper spectrum). Bottom left, Langmuir binding curve as a function of glycan concentration, used to obtain the $K_D$ ($A_{STD}$ signals correspond to *N*-acetyl protons, which are shown in the boxed area of the top panel). Bottom right, stacked STD NMR spectra as a function of $Man_5GlcNAc_2$-Asn concentration.